

At the heart of the matter: the origin of bulgeless dwarf galaxies and Dark Matter cores

F. Governato¹, C. Brook², L. Mayer³, A. Brooks⁴, G. Rhee⁵, J. Wadsley⁶, P. Jonsson⁷, B. Willman⁸, G. Stinson⁶, T. Quinn¹ and P. Madau⁹

¹Astronomy Department, University of Washington, Seattle, WA 98195, US

² Peremiah Horrocks Institute, University of Central Lancashire, Preston, Lancashire, PR1 2HE, UK

³Institute for Theoretical Physics, University of Zurich, Winterthurestrasse 190, CH-8057 Zürich.

⁴ Theoretical Astrophysics, California Institute of Technology, MC 350-17, Pasadena, CA, 91125 US

⁵Department of Physics and Astronomy, University of Nevada, Las Vegas, NV US

⁶Department of Physics and Astronomy, McMaster University, Hamilton, ON, L8S 4M1, Canada

⁷ Institute of Particle Physics, UCSC, Santa Cruz, CA 95064, US

⁸Haverford College, Department of Astronomy 370 Lancaster Ave, Haverford, PA 19041

⁹Department of Astronomy and Astrophysics. University of California, Santa Cruz, CA 95064 US

For almost two decades the properties of “dwarf” galaxies have challenged the Cold Dark Matter (CDM) paradigm of galaxy formation¹. Most observed dwarf galaxies consists of a rotating stellar disc² embedded in a massive DM halo with a near constant-density core³. Yet, models based on the CDM scenario invariably form galaxies with dense spheroidal stellar “bulges” and steep central DM profiles^{4,5,6}, as low angular momentum baryons and DM sink to the center of galaxies through accretion and repeated mergers⁷. Processes that decrease the central density of CDM halos⁸ have been identified, but have not yet reconciled theory with observations of present day dwarfs. This failure is potentially catastrophic for the CDM model, possibly requiring a different DM particle candidate⁹. This Letter presents new hydrodynamical simulations in a Λ CDM framework¹⁰ where analogues of dwarf galaxies, bulgeless and with a shallow central DM profile, are formed. This is achieved by resolving the inhomogeneous interstellar medium, resulting in strong outflows from supernovae explosions which remove low angular momentum gas. This inhibits the formation of bulges and decreases the dark-matter density to less than half within the central kiloparsec. Realistic dwarf galaxies are thus shown to be a natural outcome of galaxy formation in the CDM scenario.

In Λ CDM, the favored theory of cosmic structure formation, galaxy discs form as gas cools and collapses inside spinning halos of collisionless DM, reaching centrifugal equilibrium and turning into stars¹¹. Models which assume that the stellar component of galaxies inherits the angular momentum distribution of their host DM halos also predict the formation of a centrally concentrated stellar bulge and a cuspy DM profile^{7,12}. In contrast, the vast majority of dwarf galaxies have no stellar bulges, and the observed rotation curves of small galaxies often rise almost linearly in the central kpc, a result interpreted as a sign of a shallow DM distribution^{13,14}. This excess of low angular momentum material creates the so called "angular momentum problem"¹⁵ for CDM models.

A proposed solution to the existence of bulgeless galaxies invokes gas winds created by multiple supernovae (SN) explosions to selectively remove low angular momentum baryons from the center of galaxies¹⁶. SN winds are observed in both local and high redshift galaxies and are efficient at removing gas from the discs of nearby galaxies at a rate of few times the current star formation (SF) rate^{17,18}. Modeling the formation of a highly inhomogeneous multi phase ISM is necessary to tie SF to high density gas regions and to create SN winds able to affect the internal mass distribution of galaxies^{19,20}. Such numerical schemes for SF and resulting feedback have been applied to the formation of high redshift protogalaxies, leading to significant baryon loss and less concentrated systems^{8,20}. Similarly, dynamical arguments^{21,22} suggest that bulk gas motions (possibly SN induced) and gas clouds orbital energy loss due to dynamical friction can transfer energy to the center of the DM component. Sudden gas removal through outflows then causes the DM distribution to expand. These mechanisms were demonstrated to operate effectively in small high-redshift halos of total mass around $10^9 M_{\odot}$, where they create small DM cores⁸. However, such methods and the required high resolution have not been applied to cosmological hydrodynamical simulations of present day dwarf galaxy systems ($V_{rot} \sim 60 \text{ km s}^{-1}$). Showing that the properties of dwarf galaxies can be accurately predicted by the CDM scenario would end the "small scale crisis" and further constrain the properties of the DM particle candidate.

To study the formation of dwarf galaxies in a Λ CDM cosmology. we analyze a novel set of cosmological simulations. Baryonic processes are included, as gas cooling⁸, heating from the cosmic UV field²³, star formation and SN driven gas heating (Figure 1). Resolution is such that dense gas clumps as small as $10^5 M_{\odot}$ are resolved, similar to real SF regions¹⁹. Hence stars are allowed to form only in cold gas regions with a local density higher than 100 amu/cm^3 , reflecting typical conditions in real galaxies. This description of SF is a critical improvement over many previous cosmological simulations, where star forming regions were not individually resolved. A single dwarf galaxy (DG1) is analyzed, but we obtained equivalent results with galaxies of similar mass and different assembly histories and halo spin (another simulated galaxy is described in the supplemental material). DG1 has a rich merger history: three proto-galaxies of similar mass merge at $z \sim 3$, and a large satellite is accreted at $z \sim 1.2$ that has a mass 1/3 that of the central galaxy (a "major" merger). Several other satellites are accreted, including one at low redshift. Star formation is bursty, as observed in nearby dwarfs²⁷ peaking at $0.25 M_{\odot}/\text{yr}$ during interactions at $z \sim$

2. The disc component assembles shortly after that (Figure 1, top). At $z=0$ an exponential stellar disc is surrounded by an HI disk which extends out to six disc scale lengths. The galaxy shows no sign of a stellar spheroid (Figure 1, bottom right). The star formation rate declines after $z=1$, and by the present time it is down to $0.01 M_{\odot}/\text{yr}$, in agreement with galaxies of similar magnitude.

SN feedback creates holes in the HI distribution due to bubbles of hot gas expanding perpendicular to the disc with velocities approaching 100 km s^{-1} (Figure 1, top left). The HI super shells close to the disc plane are typically a few hundred parsecs wide, expanding at $10\text{-}30 \text{ km s}^{-1}$, similar to those observed in dwarfs²⁸. As SF happens in short, spatially concentrated bursts including several coeval star particles, the typical energy per unit mass released in the surrounding gas is sufficient to disrupt gas clouds and generate gas fountains that unbind gas from the shallow potential of the galaxy at 2-6 times the instantaneous SF rate, consistent with observations¹⁷. As predicted in earlier studies²⁰ feedback from spatially resolved SF results in a realistic low SF efficiency and a total baryon mass loss equal to a few times the final amount of stars. As star forming regions are centrally biased or rapidly sinking to the galaxy center due to dynamical friction, most of the gas becoming unbound is preferentially removed at small radii and at $z>1$.

Mock images²⁹ (Figure 1, lower panels) show that in redder bands the optical disc is relatively featureless, although star forming regions are visually associated with short lived spiral arms. The striking feature of this galaxy is the complete absence of a stellar spheroid even when observed edge-on (Figure 1). The radial light distribution in all optical and near-IR bands has an almost perfect exponential profile as observed in dwarf galaxies. This galaxy would thus be classified as “bulgeless”², i.e. lacking of a visible central stellar spheroid. The formation of a pure disc galaxy with structural properties typical of observed gas rich dwarfs²⁴ is a fundamental success of this set of simulations.

The underlying DM and baryonic mass profile of DG1 has been measured using kinematic estimators. The rotation curve of DG1 (Figure 3), was obtained measuring the rotational motion of cold ($T < 10^4 \text{ K}$) gas as a function of radius using the “tilted ring analysis”, which reproduces the effects of observational biases such as disc distortions and warping, bars and pressure support from non circular motions³⁰. The rotation curve of DG1 rises almost linearly out to one stellar disc scale length, and is still rising at four scale lengths ($\sim 4 \text{ kpc}$), similar to the rotation curves of real dwarf galaxies. This is a great success as simulations have persistently produced rotation curves which rise rapidly in the inner regions and peak inside one scale length, symptomatic of their steep central mass distributions⁵. The DM central density of DG1 has a shallow profile over a “core” of roughly 1 kpc in size (see figure 3 and Figure 5 in Supplementary Info), comparable to those measured in many dwarf galaxies^{3,13,14}. Accordingly, the DM density averaged over the same radius is $10^{7.5} M_{\odot} \text{ kpc}^{-3}$, about 50% lower than in a control run where the gas is not allowed to cool or form stars, and where the slope of the inner DM profile is instead steep as in typical DM only simulations⁶.

Outflows are the main mechanism in altering the central density profile of the baryonic

component of galaxy DG1. The strongest outflows correlate with SF bursts, caused by mergers and strong interactions, when dense gas regions form from disk instabilities and sink to the center due to dynamical friction. SN feedback destroys these gas clumps as soon as they start forming stars. Outflows then selectively remove most low angular momentum gas before it is transformed into stars, effectively quenching the processes that would lead to a concentrated baryon distribution and to the formation of stellar bulges (see Supplemental material). By the present time the angular momentum distribution of stars formed from the remaining gas has a median value higher than the DM, and lacks its low angular momentum tail (Figure 4).

The removal of centrally concentrated, low angular momentum gas is also closely connected to the origin of shallow DM profiles. As the galaxy DG1 assembles, gas starts collecting at its center via clumps and filaments while the DM remains smoothly distributed. This spatial decoupling between the gas and DM can lead to efficient orbital energy transfer from the gas to the DM through gas bulk motions⁸ and gas orbital energy loss. Additionally, the gas outflows ensuing from subsequent SF rapidly remove a large fraction of the gas, leading to a significant loss of DM binding energy, causing a net expansion and the formation of a shallow DM profile^{21,22}. Our simulations provide direct confirmation of these two mechanisms, as the expansion of the collisionless DM component occurs over several Gyrs, closely following the strongest outflows. Outflows happen both in smaller mass progenitors and then at the center of the main galaxy, where the process of core formation is essentially complete by $z \sim 0.5$ when the DM profile in the inner kpc settles to a shallow slope with $\rho \propto r^{-0.6}$, comparable to those observed and shallower than a DM-only control run that has the canonical, much steeper profile (see Figure 3 and Supplemental info).

These results predicts that low-mass, bulgeless disc galaxies should also have a shallow DM central profile and predicts that these two properties should be correlated in observed samples of nearby galaxies, as they are originated by the same physical processes.

Received ; Accepted .

-
1. Coles, P. The state of the Universe. *Nature*, **433**, 248–256 (2005).
 2. Dutton, A. On the Origin of Exponential Galaxy Discs. *Mon. Not. R. Astron. Soc.*, submitted, arXiv:0810.5164 (2008).
 3. de Blok, W. J. G., Walter, F., Brinks, E., Trachternach, C., Oh, S.-H., & Kennicutt, R. C. High Resolution Rotation Curves and Galaxy Mass Models from THINGS. *Astron. J.*, **136**, 2648–2719 (2008).
 4. Governato, F., Willman, B, Mayer, L. Brooks, A., Stinson, G., Valenzuela, O., Wadsley, J. and Quinn, T. Forming disc galaxies in Λ CDM simulations. *Mon. Not. R. Astron. Soc.*, **374**, 1479–1494 (2007)

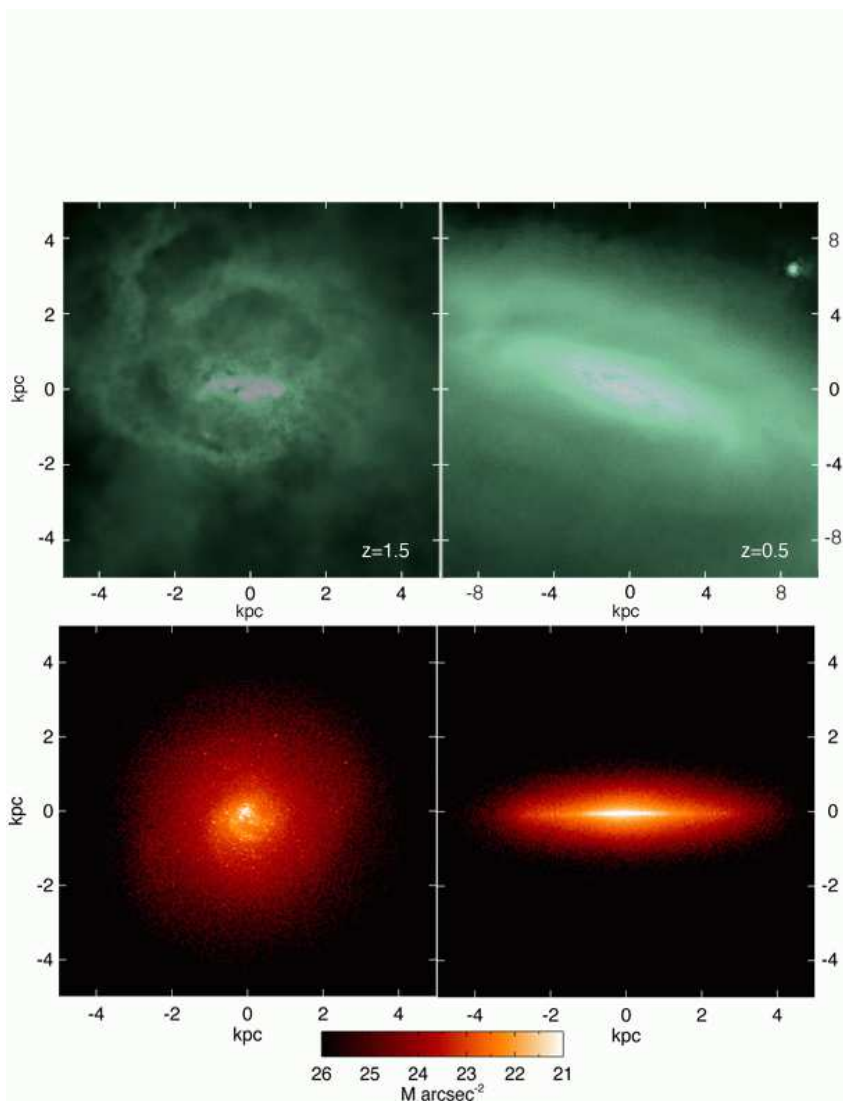


Figure 1. The observable properties of simulated galaxy DG1. Top Left: Colour-coded density map of the gas distribution at $z=1.5$, showing the gas outflows and super shells. Top Right: The gas distribution at $z=0.5$ when the disc has fully formed (note the larger scale). At $z=0$ the total mass of the system within the virial radius is $3.5 \times 10^{10} M_{\odot}$. As a result of outflows and inefficient star formation, the disk (including HI gas and stars) to virial mass ratio is only $f_{disk} = 0.04$, 70% of the disk mass is in HI, and the M_{HI}/L_B ratio is 1.2. The amount of baryons within the virial radius is only 30% of the cosmic fraction. These values are consistent with those observed in real galaxies of similar mass⁷. Bottom Left: The face on light distribution at $z=0$ in the SDSS i band. Bottom Right: The galaxy seen edge on in the same band. The effect of dust absorption is included. The total magnitude of the galaxy in the i SDSS band is -16.8 giving an i band M/L ratio of ~ 20 . The galaxy $g-r$ colour is 0.52, typical of star forming dwarf galaxies²⁴. The rotation velocity is $\sim 55 \text{ km s}^{-1}$, as measured using the $W_{20}/2$ line width of the HI distribution. This simulation resolves the internal structure of galaxy DG1 with several million resolution elements, achieves a mass resolution of $10^3 M_{\odot}$ for each star particle and a force resolution of 86pc. In the supplementary material we show that high resolution coupled with SF being spatially associated to small gas clouds is a fundamental requirement for SN feedback to originate outflows and lower the density at the center of galaxy halos. Simulations using the same implementation of SF and feedback reproduce some global scaling properties of observed galaxies across a range of masses and redshifts^{25,26}.

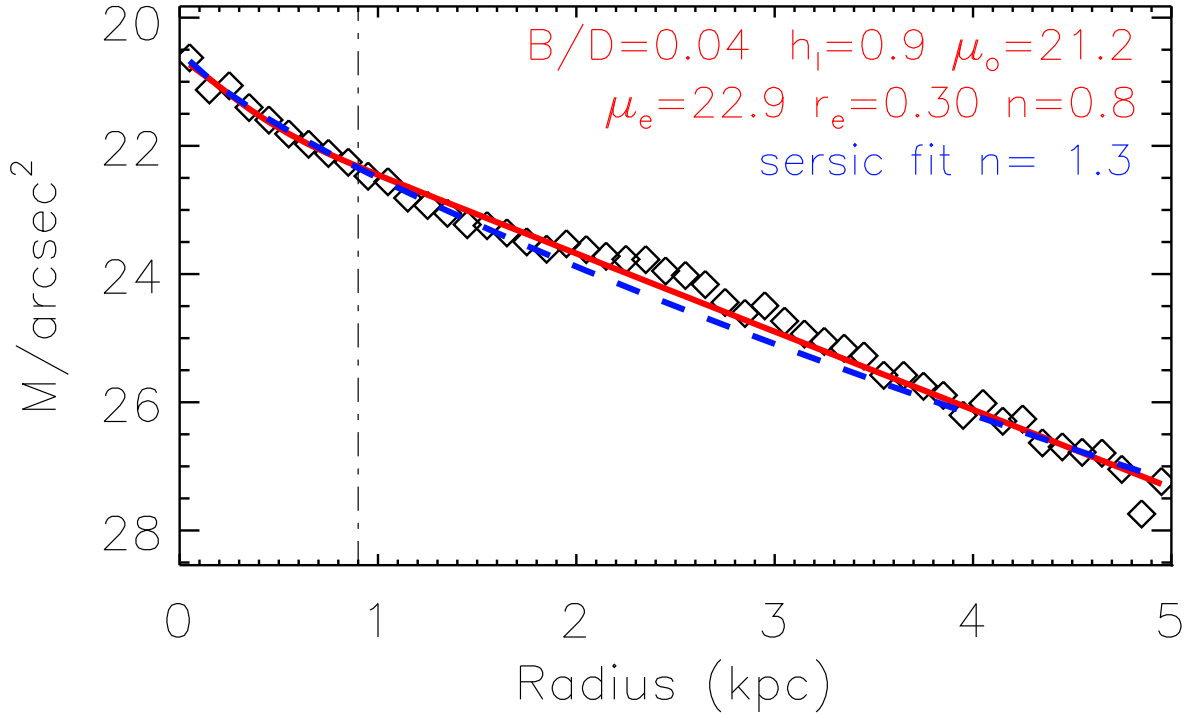


Figure 2. The SDSS i -band radial light profile of the simulated dwarf galaxy DG1 at $z=0$. Being less sensitive to recent star formation events, the i band is commonly used to describe the underlying stellar mass distribution. The galaxy has an almost pure exponential disc-like light profile (diamonds), with a formal bulge+disc fit to the 2D light distribution giving a B/D ratio of 0.04 as seen face on. The measured disc scale length is 0.9 kpc (dot dashed vertical line). The dashed and continuous lines show the Sersic+exponential fit to the disc and a one component Sersic profile fit with $n=1.3$. An index value of $n<1.5$ identifies bulgeless disc galaxies in large surveys^{2,3}. The galaxy would then be classified as “bulgeless”. Images in other optical bands and the near-IR K band give a similar fit with extremely low B/D ratios. Fits were measured using the public software GALFIT and a 1D two-component fitting procedure, obtaining similar results. A second galaxy (DG2), shows a profile best fit by a pure exponential, with a Sersic index of one (see Figure 6 in Supplementary info and references there). Images were created using SUNRISE²⁹, which creates spectral energy distributions using the ages and metallicities of each simulated star particle, and takes into account the full 3D effects of dust re-processing.

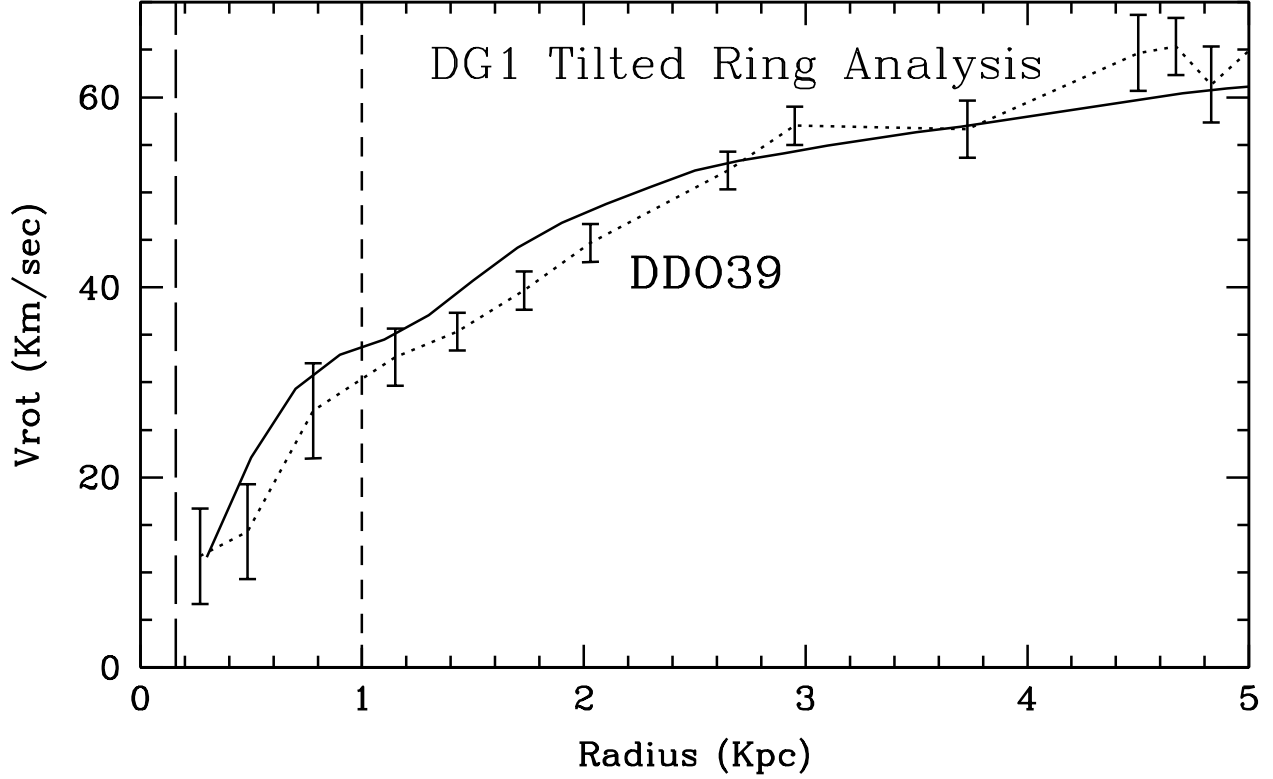


Figure 3. The rotation curve of the simulated dwarf compared to that measured for a real galaxy. The continuous black line shows the rotation velocity of the galaxy using actual projected velocity field and the tilted ring analysis³⁰ (see Supplemental Info). The dotted line shows the rotation curve of the galaxy DDO39 as measured using a similar technique¹⁴, with standard deviation error bars. The velocity profile of both the observed and simulated galaxies imply a DM distribution with a core scale length of about 1 kpc, as directly measured in the simulation (Fig.5 in the Supplemental Info). The long dashed vertical line shows the force resolution of the simulation, while the dashed vertical line marks the approximate scale length of the DM “core”. The underlying DM density $\rho_{DM} \propto r^\alpha$, with $\alpha=-0.6$ in the central kpc, is consistent with observational estimates and shallower than a DM only simulation (see Supplemental info) that would predict a steeper profile with $\alpha = -1.3$

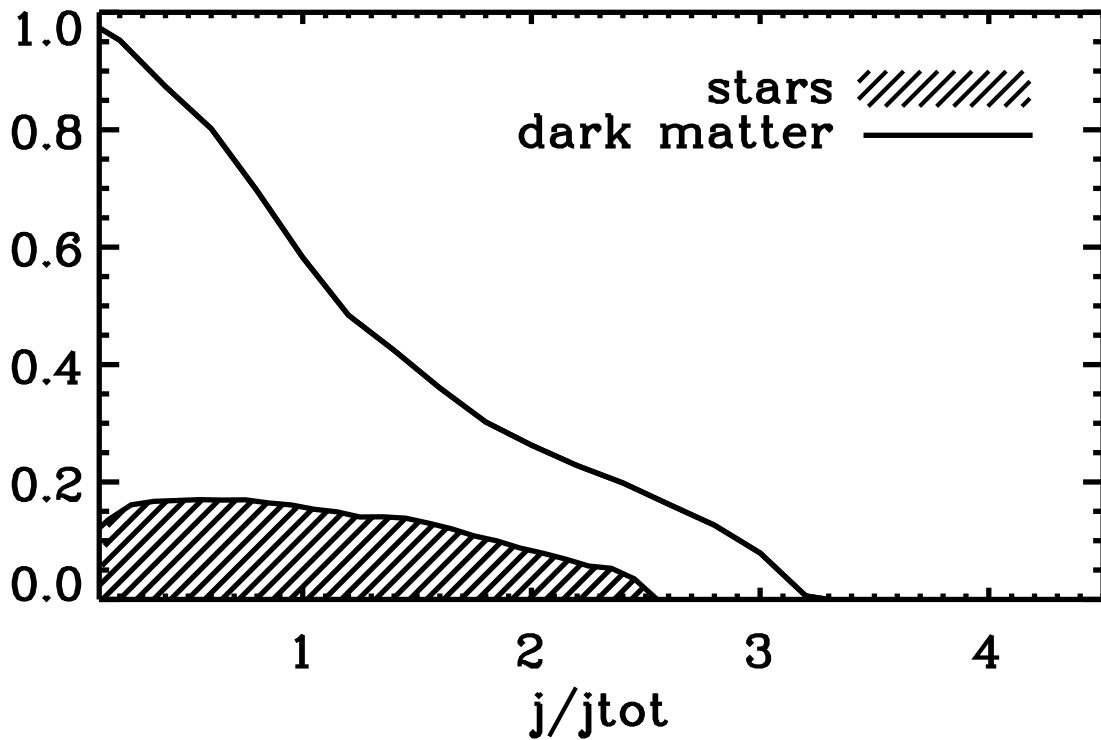


Figure 4. A comparison between the angular momentum distribution of the stellar disk and the dark matter halo in the simulated galaxy DG1. The panel shows the present day time angular momentum distribution of disc stars (shaded area) and DM particles (area below the continuous line) normalized by the median value for the whole DM halo ($j_{\text{tot}}=1$). The angular momentum distribution of star particles has a narrower distribution, a higher average and significantly less low angular momentum material than the DM, due to centrally concentrated outflows preferentially removing low angular momentum baryons. As a result, the radial stellar distribution is similar to that measured for normal dwarf galaxies^{2,3} (see also Figure 2).

5. Abadi, M. G., Navarro, J. F., Steinmetz, M. and Eke, V. R., Simulations of Galaxy Formation in a Λ Cold Dark Matter Universe. I. Dynamical and Photometric Properties of a Simulated Disk Galaxy *Astrophys. J.*, **591**, 499-514 (2003)
6. Moore, B., *et al.*, Cold collapse and the core catastrophe, *Mon. Not. R. astron. Soc.* **310**, 1147-1152 (1999)
7. van den Bosch, F. C., Burkert, A., & Swaters, R. A., The angular momentum content of dwarf galaxies: new challenges for the theory of galaxy formation *Mon. Not. R. Astron. Soc.*, **326**, 1205– (2001)
8. Mashchenko, S., Wadsley, J. and Couchman, H., M. P Stellar Feedback in Dwarf Galaxy Formation. *Science*, **319**, 174–177 2008
9. Primack, J. Cosmology: small scales issues revisited. 2009 arXiv:0909.2247 Invited contribution to NJP Focus Issue on Dark Matter and Particle Physics.
10. Spergel, D. N. *et al.* First-year Wilkinson Microwave Anisotropy Probe (WMAP) observations: determination of cosmological parameters. *Astrophys. J. Suppl.*, **148**, 175–194 (2003).
11. Fall, S. M. and Efstathiou, G., Formation and Evolution of disc galaxies with haloes. *Mon. Not. R. Astron. Soc.*, **193**, 189–206 (1980)
12. Barnes, J. E and Hernquist, L. Transformations of Galaxies. II. Gasdynamics in Merging Disk Galaxies. *Astrophys. J.*, **471**, 115. (1996)
13. Simon, J. D., Bolatto, A. D., Leroy, A., Blitz, L. and Gates, E. L. High-Resolution Measurements of the Halos of Four Dark Matter-Dominated Galaxies: Deviations from a Universal Density Profile. *Astrophys. J.* **621**, 757–776 (2005)
14. Swaters, R. A., Verheijen, M. A. W., Bershady, M. A. and Andersen, D. R. The Kinematics in the Core of the Low Surface Brightness Galaxy DDO 39 *Astrophys. J. Lett.*, **587**, L19-L22 (2003)
15. Maller, A. H., Dekel, A. Towards a resolution of the galactic spin crisis: mergers, feedback and spin segregation. *Mon. Not. R. Astron. Soc.* **335** 487–498 (2002)
16. Binney, J., Gerhard, O. and Silk J. The dark matter problem in disc galaxies. *Mon. Not. R. Astron. Soc.*, **321**, 471–474 2001.
17. Martin, C. L. Properties of Galactic Outflows: Measurements of the Feedback from Star Formation. *Astrophys. J.*, **513**, 156–160 1999
18. Wilman, R. J., Gerssen, J., Bower, R. G., Morris S., L., Bacon, R., de Zeeuw, P. T. and Davies, R.L. The discovery of a galaxy-wide superwind from a young massive galaxy at redshift $z \sim 3$. *Nature*, **436**, 227–229 2005.
19. Robertson, B. and Kravtsov, A. Molecular Hydrogen and Global Star Formation Relations in Galaxies. *Astrophys. J.* **680**, 1083–1111 2008
20. Ceverino, D. and Klypin, A. The role of stellar feedback in the formation of galaxies. *Astrophys. J.* in press 2009.

21. Mo, H. J. and Mao, S. Galaxy formation in pre-processed dark haloes. *Mon. Not. R. Astron. Soc.*, **353**, 829-840, 2004.
22. Mashchenko, S., Couchman, H. M. P., and Wadsley, J. The removal of cusps from galaxy centres by stellar feedback in the early Universe. *Nature*, **442**, 539, 2006.
23. Haardt, F. & Madau, P., Radiative Transfer in a Clumpy Universe. II. The Ultraviolet Extragalactic Background. *Astrophys. J.* **461**, 20-37(1996)
24. Geha, M., Blanton, M. R., Masjedi, M. and West, A. A. The Baryon Content of Extremely Low Mass Dwarf Galaxies. *Astrophys. J.*, **653**, 240-254 (2006).
25. Brooks, A., Governato, F., Booth, C. M., Willman, B., Gardner, J. P., Wadsley, J., Stinson, G. and Quinn, T. The Origin and Evolution of the Mass-Metallicity Relationship for Galaxies: Results from Cosmological N-Body Simulations. *Astrophys. J. Lett.*, **655**, L17-20 2007
26. Pontzen, A., Governato, F., Pettini, M., Booth, C. M., Stinson, G., Wadsley, J., Brooks, A. and Quinn, T. Damped Lyman α systems in galaxy formation simulations. *Mon. Not. R. Astron. Soc.*, **390**, 1349-1371, 2008
27. Lee, J. C., Kennicutt, R. C., José G. Funes, S. J., Sakai, S. and Akiyama, S. Dwarf Galaxy Starburst Statistics in the Local Volume. *Astrophys. J.*, **692**, 1305–1320, 2009
28. Walter, F. and Brinks, E., Holes and Shells in the Interstellar Medium of the Nearby Dwarf Galaxy IC 2574. *Astron. J.*, **118**, 273–301, 1999
29. Jonsson, P. SUNRISE: polychromatic dust radiative transfer in arbitrary geometries, *MNRAS*, **372**, 2-20 (2006)
30. Valenzuela, O., Rhee, G., Klypin, A., Governato, F., Stinson, G., Quinn, T. and Wadsley, J. Is There Evidence for Flat Cores in the Halos of Dwarf Galaxies? The Case of NGC 3109 and NGC 6822. *Astrophys. J.*, **657**, 773-789 (2007).

Supplementary Information is linked to the online version of the paper at www.nature.com/nature

Acknowledgments We acknowledge discussions with L. Blitz, A. Kravtsov, J. Primack, I. Trujillo and V. Wild. We thank R. Swaters and the THINGS team for sharing some of their data with us. LM was supported by a grant of the Swiss National Science Foundation. LM and CB thank the Kavli Institute for Theoretical Physics at UC Santa Barbara for hospitality during the early stages of this work. FG and PM thank the computer support people at Nasa Advanced Supercomputing, TERAGRID, ARSC, and UW, where the simulations were run.

Author Information Reprints and permissions information is available at npg.nature.com/reprintsandpermissions. The authors declare no competing financial interests.

Correspondence and requests for materials should be addressed to F.G. (fabio@astro.washington.edu).

SUPPLEMENTARY INFORMATION

This is an extension of the Letter to Nature, aimed at providing further details, in support of the results reported in its main body.

1 The SPH Treecode Gasoline

We have used the fully parallel, N-body+smoothed particle hydrodynamics (SPH) code GASOLINE to compute the evolution of both the collisionless and dissipative component in the simulations. A detailed description of the code is available in the literature³¹. Here we recall its essential features. GASOLINE computes gravitational forces using a tree-code³² that employs multipole expansions to approximate the gravitational acceleration on each particle. A tree is built with each node storing its multipole moments. Time integration is carried out using the leapfrog method, which is a second-order symplectic integrator requiring only one costly force evaluation per timestep and only one copy of the physical state of the system. In cosmological simulations periodic boundary conditions are mandatory. GASOLINE uses a generalized Ewald method³³ to arbitrary order, implemented through hexadecapole.

SPH is a technique of using particles to integrate fluid elements representing gas^{34,35}. GASOLINE is fully Lagrangian, spatially and temporally adaptive and efficient for large N . The version of the code used in this Letter includes radiative cooling and accounts for the effect of a uniform background radiation field on the ionization and excitation state of the gas. The cosmic ultraviolet background is implemented using the Haardt-Madau model²³, including photoionizing and photoheating rates produced by PopIII stars, QSOs and galaxies starting at $z = 9$. The assumption that reionization occurred at high z is consistent with the combination of the 3rd year WMAP results and the Gunn-Peterson effect in the spectra of distant quasars³⁶. We use a standard cooling function for a primordial mixture of atomic hydrogen and helium at high gas temperatures, but we include the effect of metal cooling⁸ and evolving gas metallicities below 10^4 K (the metallicity in dwarfs is indeed much lower than solar³⁷, with $-1 < [Fe/H] < -2$). The internal energy of the gas is integrated using the asymmetric formulation, that gives results comparable to the entropy conserving formulation³⁸ but conserves energy better. Dissipation in shocks is modeled using the quadratic term of the standard Monaghan artificial viscosity³⁵. The Balsara correction term is used to reduce unwanted shear viscosity³⁹.

In the simulations described in this Letter star formation occurs when cold gas reaches a given threshold density^{40,41} typical of actual star forming regions (we used 100 amu/cm^3 in most runs and discuss the effect of a lower threshold in §5). SF then proceeds at a rate proportional to $\rho_{gas}^{1.5}$, i.e. locally enforcing a Schmidt law. The adopted feedback scheme is implemented by releasing energy from SN into the gas surrounding each star particle⁴¹. The energy release rate is tied to the time of formation of each particle (which effectively ages as a single stellar population with a Kroupa IMF). To model the effect of feedback at unresolved scales, the affected gas has its cooling shut off for a time scale proportional to the Sedov solution of the blastwave equation, which is set by the local density and temperature

of the gas and the amount of energy involved. In the high resolution runs described in this study this translates into regions of ~ 0.1 to 0.3 kpc in radius being heated by SN feedback and having their cooling shut off. At $z > 1$ the affected gas has its cooling shut off for typically 5-10 million years. However, even during high z starbursts only a few per cent of the gas in the disc plane has a temperature $T > 40,000$ Kelvin. The effect of feedback is to regulate star formation in the discs of massive galaxies and to greatly lower the star formation efficiency in galaxies with peak circular velocity in the $50 < V_c < 150$ km s^{-1} range²⁵. At even smaller halo masses ($V_c < 20\text{-}40$ km s^{-1}) the collapse of baryons is largely suppressed by the cosmic UV field^{25,42}. Other than the density threshold only two other parameters are needed, the star formation efficiency ($\epsilon\text{SF} = 0.1$) and the fraction of SN energy coupled to the ISM ($e\text{SN}=0.4$). Similar values have been used in previous works by this group⁴. However, here we slightly increased ϵSF from 0.05 to 0.1 to ensure a better normalization to the radial Schmidt law. We explored values of $e\text{SN}$ as high as 0.6 and cooling shutoff times changing by a factor of a few, verifying that, in the mass range of this study, mass profiles and SF histories are relatively insensitive to longer (shorter) cooling shutoff timescales if a smaller (larger) fraction of SN energy is coupled to the ISM.

2 Initial Conditions: Cosmological volume and the adopted cosmology

At $z = 0$ the virial mass of the halos that we studied in this Letter are 3.5 (DG1) and 2.0 (DG2) $\times 10^{10} M_\odot$ (the virial mass is measured within the virial radius R_{vir} , the radius enclosing an overdensity of 100 times the cosmological critical density). The halos were selected within a large scale, low resolution, dark matter only simulation run in a concordance, flat, Λ -dominated cosmology: $\Omega_0 = 0.24$, $\Lambda=0.76$, $h = 0.73$, $\sigma_8 = 0.77$, and $\Omega_b = 0.042$ ^{10,43}. The size of the box, 25 Mpc, is large enough to provide realistic torques for the small galaxies used in this work. The power spectra to model the initial linear density field were calculated using the CMBFAST code to generate transfer functions.

3 Volume renormalization technique

The simulations described here require a large dynamical range, from sub-kpc scales to correctly describe the internal dynamics of the dwarf galaxies, to several tens of Mpc to include the effects of cosmic torques from the large scale structure. This is achieved by the volume renormalization (or “zoom in”) technique⁴⁴. From the $z=0$ output of the large scale simulation the regions of interest where each galaxy forms were identified and traced back to a Lagrangian sub region in the initial conditions. Then the initial conditions are reconstructed using the same low-frequency waves present in the low resolution simulation but adding the higher spatial frequencies. The power spectrum is realized by using Fast Fourier Transforms (FFTs) to determine displacements of particles from this grid. We use a particular technique that allows one to calculate high resolution FFTs only in the regions of the simulations where mass and force resolution need to be high. To reduce the number of particles and make the full N-Body + SPH simulation possible with the same cosmological context, we construct initial conditions where the mass distribution is

sampled at higher resolution (less massive particles on a finer grid) and then more coarsely as the distance from the chosen object increases. Dark matter particle masses in the high resolution regions are $1.6 \times 10^4 M_{\odot}$, and the force resolution, i.e., the gravitational softening, is 86 pc (more details in Table 1). In total, at $z=0$ there are 3.3×10^6 particles within the virial radius of galaxy DG1. For all particle species, the gravitational spline softening, $\epsilon(z)$, was evolved in a comoving manner from the starting redshift ($z \sim 100$) until $z=8$, and then remained fixed at its final value from $z=8$ to the present. The softening values chosen are a good compromise between reducing two body relaxation and ensuring that disc scale lengths and the central part of dark matter halos will be spatially resolved. Integration parameter values were chosen according to the results of previous systematic parameter studies⁴⁵. This technique achieves CPU savings of several orders of magnitude, since running the original volume at the same resolution of the central region would have required more than 30 billion particles. This method has been successfully used in a wide range of cosmological studies^{4,25,46} that have shown how the assembly history of the “zoomed-in” objects is preserved when compared to the original version in the low resolution volume.

4 The Photometric and Kinematic Analysis

To properly compare the outputs from the simulation to real galaxies and make accurate estimates of the *observable* properties of galaxies, we used the Monte Carlo radiation transfer code *SUNRISE*^{29,47} to generate artificial optical images (see Figure 1 and 6) and spectral energy distributions (SEDs) of the outputs of our run. *SUNRISE* allows us to measure the dust reprocessed SED of every resolution element of the simulated galaxies, from the far UV to the far IR, with a fully 3D treatment of radiative transfer. Filters mimicking those of the SDSS survey⁴⁸ are used to create mock observations. The 2D light profiles are then fitted as the superposition of a Sersic and an exponential component using the widely used program GALFIT⁴⁹. Results were compared with a two component, radially averaged 1D routine developed by the authors, finding similar results.

The model galaxy rotation curves (Figure 3) were determined using the standard tilted-ring analysis⁵⁰ that is applied to galaxy observations. The idea behind this is to facilitate a comparison between galaxy models and observations by deriving rotation curves for both using the same methods. The assumption is that a rotating disc galaxy can be described by a set of concentric rings. Each ring has a constant circular velocity and two orientation angles. The values of the ring parameters are determined from the observed radial velocities in a set of concentric elliptic annuli. For each ring we determine the intensity weighted velocity along the line of sight at each pixel on the annulus and compute the rotational velocity of the gas at each annulus. The method has been recently applied to model galaxies⁵¹ to study the effect of systematic biases due to non circular motions in the measured rotation curves of real galaxies⁵².

5 Resolution tests and cosmic variance

Recent work has highlighted the role of numerical resolution and different SF and feedback implementations in driving the structural properties of simulated galaxies and specifically their internal mass distribution^{53,54,55}. To demonstrate the robustness of our results analyse one of our galaxies (DG1) at lower resolutions, and a different galaxy with a different merger history (DG2), but similar mass and halo spin ($\lambda \sim 0.05$ ⁵⁶), and show that our key results are produced in these simulations a) independently of the assembly history of the parent halo, b) when the spatial and force resolution are sufficiently high and c) when SF is spatially resolved, meaning that it happens only in cold gas particles dense enough to be representative of star forming regions, i.e. with density higher than 100 atom/cm^3 .

The parameters of the analysed galaxies are summarized in Table 1, where the galaxy described in the main section of the Nature Letter is DG1, its lower resolution versions using the same initial conditions are DG1MR and DG1LR, and a version using a lower density threshold (0.1 amu/cm^3) for star formation is DG1LT (it has the same resolution as DG1MR). DG1DM is a run using the same initial conditions but including only the dark matter component. DG2 has the same mass and spatial resolution as DG1. Each run was completed following the guidelines described in the Initial Conditions section. The structural properties of the galaxies are measured using techniques that mimic observations and are presented in Table 2.

As shown in Figure 5, poor resolution and an inconsistent implementation of star formation affect the global mass distribution of galaxies, leading to overly dense central regions. The rotational velocities based on the local 3D potential (and assuming circular orbits) for different DG1 realizations and for DG2 are plotted in the left panel of Figure 5. Convergence is apparent in DG1 and DG1MR (particles in the DG1MR run are 2.3 times more massive). DG2, which has a final mass slightly smaller than DG1, also has a velocity profile that keeps raising for several kpcs. As a further test, we verified that the DM only run (DG1DM) has a DM profile similar to what obtained in previous, similar simulations⁵⁷, with a central DM density proportional to r^α , with $\alpha \sim -1.3$. The above result shows that in our high resolution simulations the mass distribution of the galaxies presented in this Letter is free from numerical effects.

Instead, the low resolution run DG1LR forms a galaxy much more centrally concentrated. This run adopts the *same* SF criteria and feedback scheme as the higher resolution counterparts, but uses 64 times less particles than DG1 (force resolution is also 4 times worse, 350pc). DG1LR has a flat, rather than rising rotation curve. As we have shown in previous works, its low resolution causes enhanced angular momentum loss in the baryonic component via a variety of numerical effects⁵³. These numerical effects come from the low number of resolution elements and exist irrespective of the modeling of the ISM and of the threshold density used for star formation. Moreover, at the resolution of DG1LR, a single gas particle has the mass of a SF region ($10^{5-6} M_\odot$). As individual density peaks are unresolved, SF only happens at the very center of the galaxy, further increasing the final central density of baryons and DM.

Similarly, to show how resolution, details of SF and outflows specifically affect the DM density profile, the various realizations of DG1 and DG2 are shown in the right panel of Figure 5. DG1, the main simulation described in the Nature Letter is in blue, while the medium resolution simulation is in red, again showing shallow central DM profiles and clear convergence at our maximum resolution. DG2 has a shallow profile as well. On the contrary, the dot dashed black line shows the steep central profile of DG1DM, the DG1 dark matter only simulation, and highlights the degree to which the DM profile is flattened by processes connected to the baryonic component.

In our high resolution simulations, where $T_{min} \sim 500\text{K}$ we resolve the local Jeans length implied by the high density threshold with at least 2 SPH kernels, thus preventing artificial fragmentation⁵⁸ as visually evident in the top right panel of Figure 1, showing a smooth gaseous disc. In DG1LR the resolution would not be enough to resolve the local Jeans length at the high density threshold, but the large gravitational softening (larger than both the smoothing length and the Jeans length) has a dominant effect, suppressing artificial fragmentation. Hence none of our runs suffers from artificial fragmentation and any clumpiness present is to be regarded as physical.

It is important to highlight that the the mass distribution of galaxy DG2 is similar to DG1, as the rotation curve is linearly rising for several scale lengths and the DM profile shows a shallow central region of about one kpc in radius. In panels a and b of Figure 6, we plot the face and edge on surface brightness maps of DG2, and the resulting *i*-band surface density profile in panel c. Clearly, the profile is a pure exponential all the way to the center. A two component fit gives $B/D=0.01$, and a fit with a Sersic profile yields an index of 1, corresponding to a pure exponential disc. At difference with DG1, DG2 has a quiet merging history with fewer major mergers and only very minor accretion events after $z \sim 1.5$, showing that the suppression of bulge formation and a flat central DM profile depend more on the strength of feedback rather than on cosmic variance and the details of the recent assembly history of a given galaxy.

6 Inhomogeneous ISM, the removal of low angular momentum gas and the expansion of the central DM distribution

Several analytical and numerical papers have highlighted the necessity of resolving a clumpy multi-phase ISM to achieve a realistic modeling of energy deposition in the central regions of galaxies. While using a variety of arguments, these works suggest that only in a clumpy ISM is it possible to a) transfer orbital energy from gas to the DM as dense clumps sink through dynamical friction or resonant coupling^{8,16,21,22,59,60} and have b) efficient gas outflows^{15,54}. In turn, these outflows 1) suppress the formation of stellar bulges by removing negative or low angular momentum gas^{7,15,16,21} and 2) make the central DM expand by suddenly reducing the total enclosed mass and reducing the DM binding energy²¹. However, none of the above works has simultaneously studied the formation of bulgeless galaxies and that of DM cores, even if they both are crucial properties of small galaxies.

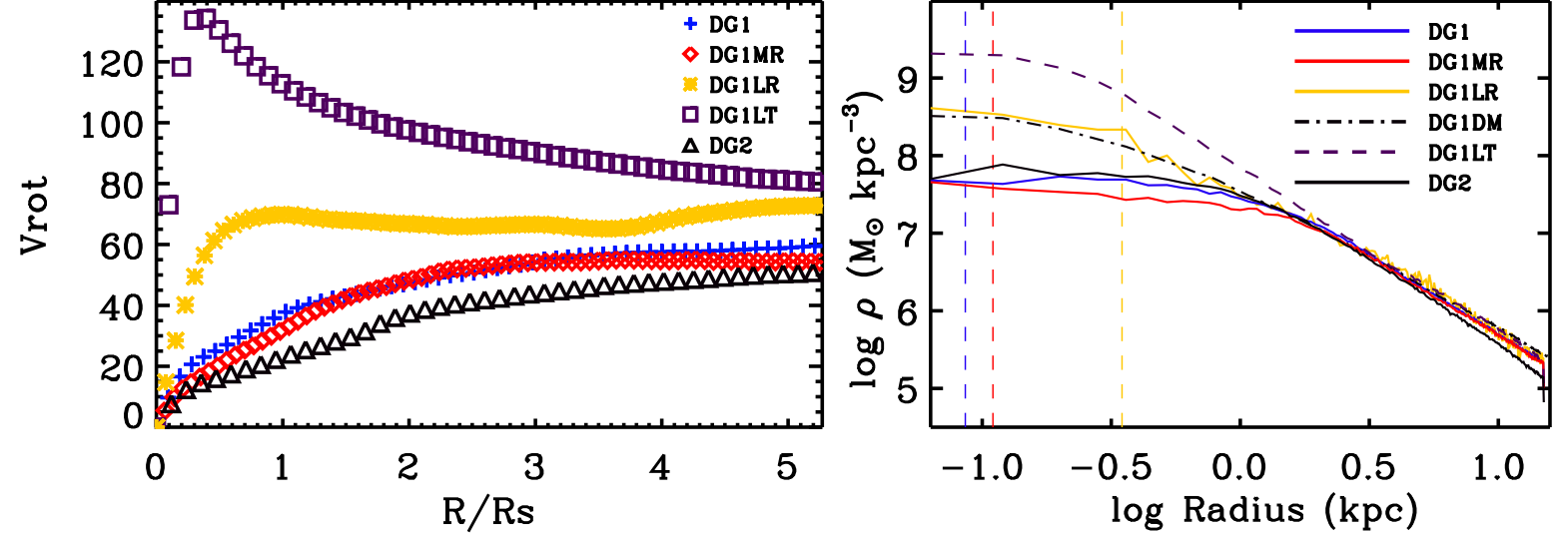


Figure 5. The rotation curve and DM radial distribution of the models described in §3 and §5, to show the effects of resolution and different SF recipes on the central mass distribution of simulated dwarf galaxies. The left panel shows the rotation curve, derived using the 3D potential of each galaxy and measured at $z=0$, for DG1 (blue crosses), DG1MR (red diamonds) and DG1LR, (yellow stars), plotted versus the disc scale length (1kpc for DG1, 0.5kpc for DG2). The three runs use the same gas density threshold for SF (100 atoms/cm^3), but MR and LR runs use only 40% and 12.5% of the particles of the reference run (with particle masses rescaled to the same total mass), and a softening respectively 1.33 and 4 times larger. Results have converged at the DG1MR resolution, while the LR run shows an excess of central material that is due to poor resolution causing artificial angular momentum loss⁵³. The squares show DG1LT, where star formation is allowed in regions with a much lower local density (0.1 atoms/cm^3), again resulting in a much higher central mass density, due to the lack of outflows. This result demonstrates that the correct modeling of where SF is allowed to happen (namely only in gas with density comparable to that of real star forming regions) is crucial to obtain the results described in this Letter. The rotation curve of galaxy DG2 (black triangles) shows the same shape as that of the DG1 run. Panel B uses a similar colour scheme and plots the DM density profile for the same runs. DG1 (blue solid), DG1MR (red dashed) show similar profiles, with a DM core of about 1kpc. Color coded vertical lines mark the force resolution for each run. The DM only run DG1DM (dot dashed), shows instead a cuspy profile down to the force resolution (red dashed vertical line as for DG1MR). The central density is about 10 times higher than in the runs with strong outflows. DG2 has a similar profile to DG1, while the lower resolution run or the run with diffuse SF have dense and cuspy DM profiles down to the force softening length.

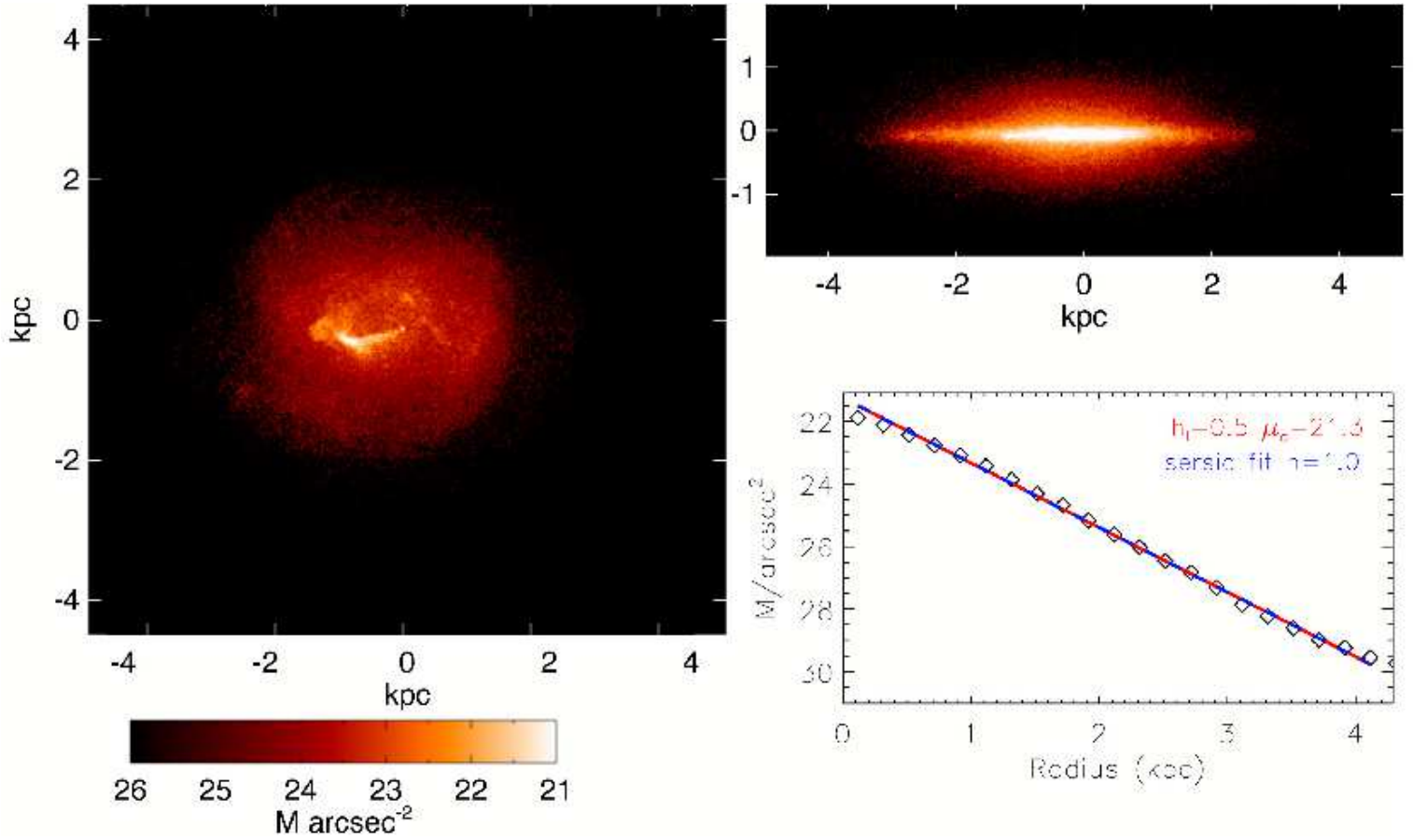


Figure 6. The optical properties of simulated galaxy DG2. Clockwise from left: The dust reddened *i*-band surface brightness map of galaxy DG2 seen face-on, edge-on, and the 1D radial surface brightness profile. The radial profile shows that the simulated galaxy is “bulgeless,” with an almost perfect exponential profile with a scale length of 0.5 kpc. (the Sersic profile with $n=1$ is equivalent to an exponential profile).

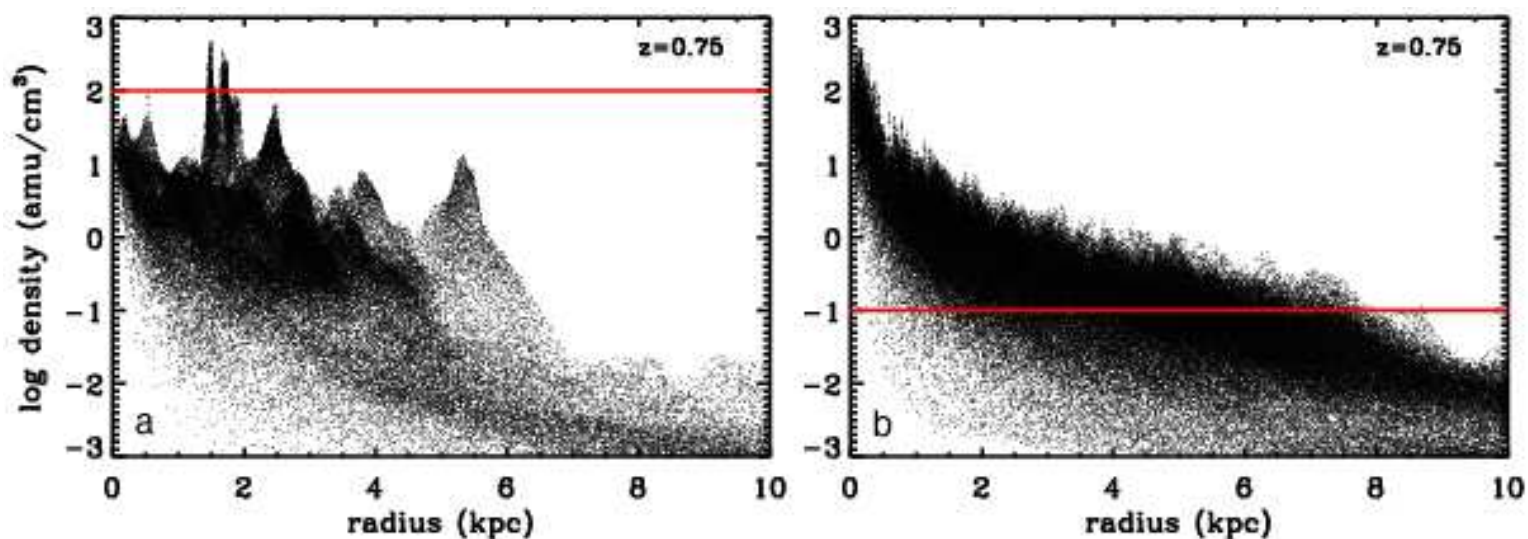


Figure 7. Properties of the gas distribution for different SF implementations. The local gas density measured around each SPH particle is plotted as a function of its radial distance from the galaxy center for runs DG1MR and DG1LT, which have identical force and mass resolution, but differ in the star formation density threshold. Horizontal red lines mark the minimum gas density for SF in each run. In both runs the SFR is $\propto \rho_{gas}^{1.5}$. In the low threshold simulation, diffuse star formation in the inner regions continues unabated by feedback, as SN energy is more evenly distributed and is unable to originate major outflows. Allowing star formation only in high density regions results in a complex, inhomogeneous ISM, even in the central regions and fast outflows that remove gas preferentially from the galaxy center.

Run	DM Part. Mass M_{\odot}	Gas Part. Mass M_{\odot}	Force Resol. (pc)	Redshift $_{LMM}$ z	Stellar Mass M_{\odot}	SF
DG1	1.6e4	3.3e3	86	1.	4.8e8	High Th.
DG1MR	3.7e4	7.8e3	116	1.	5.0e8	High Th.
DG1LR	1e6	2.1e5	350	1.	4.8e8	High Th.
DG1LT	3.7e4	7.8e3	116	1.	3.7e9	Low Th.
DG1DM	2e4	-	86	1.	-	-
DG2	1.6e4	3.3e3	86	2.	1.8e8	High Th.

Table 1. Summary of the main numerical parameters for each simulation described in §3 and §5. From left: DM and gas particle masses, force resolution, redshift of the last major merger, galaxy stellar mass at $z=0$ and the SF model adopted. The high resolution DG1 and DG2 galaxies have a total virial mass of 3.5 (2.0) $10^{10} M_{\odot}$ respectively. They both have a λ spin parameter⁵⁶ of 0.05. The highest resolution version of DG1 has about 3.5 million particles within the virial radius.

In order to achieve a multi phase ISM numerical works agree that a minimal spatial resolution of about 100pc is required, and that SF has to be associated with dense regions with gas density (~ 100 amu/cm³)^{40,61}. Our simulations satisfy both conditions and unify the many proposed models that focused on different aspects of the problem to robustly demonstrate that energy transfer and subsequent baryon removal are concurrent and effective to create bulgeless galaxies with a shallow DM profile in a full cosmological setting.

To illustrate the clumpiness of the ISM in our simulations, Figure 7 highlights the differences in the density distribution of the interstellar medium between the simulations DG1MR and DG1LT, by plotting the local gas density vs radius of each gas particle at a representative epoch of $z=0.75$. These two runs have the same mass and spatial resolution and adopt identical feedback schemes. They only differ in the way regions where SF happens are selected. In the “high threshold” runs (DG1,DG2 DG1MR and DG1LR) SF happens only in regions above a high gas density threshold (100 amu/cm³, the horizontal red line in the left panel of Figure 7). The density peaks then correspond to isolated clumps of cold gas with masses and sizes typical of SF regions. The efficiency of SF, ϵ_{SF} , for these regions must be increased from 0.05 (LT) to 0.1 (HT) in order to match the observed normalization of SF density in local galaxies. However, due to the increased densities, at any given moment only a few regions are actively forming stars. These star forming regions get disrupted after the first SNe go off and only a small fraction of gas has been turned into stars. Feedback then creates an ISM with cold filaments and shells embedded in a warmer medium. This patchy distribution allows the hot gas to leave the galaxy perpendicular to the disk plane at velocities around 100 km s⁻¹. Rather than developing a clumpy ISM as in the “high threshold” case, SF in the “low threshold” scheme is spatially diffuse (Figure 7). This means that SN energy is more evenly deposited onto the gas component, but less overall gas is effected by SN feedback due to the low densities in the SF regions. By monitoring where SN energy is deposited and where gas gets substantially heated at high

Run	M_i	$g-r$	SFR M_\odot/yr	R_s kpc	V_{rot} km/s	M_{HI}/L_B
DG1	-16.8	0.52	0.01	0.9	56	1.2
DG1MR	-16.9	0.54	0.02	0.9	55	1.0
DG1LR	-18.7	0.33	0.22	0.9	62	0.64
DG1LT	-19.4	0.40	0.38	1.3	78	0.11
DG2	-15.9	0.46	0.02	0.5	54	2.8

Table 2. Summary of the observable properties of the different dwarf runs. the SFR is in M_\odot/yr , R_s is the disc scale length, V_{rot} is measured using the HI velocity field as $W_{20}/2$

instantaneous rates, we verified that in the “high threshold” case a larger mass of gas achieves temperatures higher than the virial temperature ($T_{vir} \sim 10^5$ K) per unit mass of stars formed than in the “low threshold” scheme. Since less mass is affected in the “low threshold” scenario, the outflows are weak compared to the “high threshold” case. By $z=0$ DG1LT has formed ten times more stars, most of them in the central few kpcs, causing strong adiabatic contraction of the DM component. Its light profile is consistent with a B/D ratio of 0.3, typical of much more massive galaxies and more concentrated than in real dwarfs.

We note that in the runs adopting the “high threshold” SF, feedback produces winds that are comparable in strength to those happening in real galaxies of similar mass. However, in our simulations the cold ISM is still only moderately turbulent (~ 10 km s^{-1} at $z=0$), consistent with observations⁶², and the galaxies match the observed stellar and baryonic Tully Fisher relation⁶³, as the SF efficiency is regulated to form an amount of stars similar to that of real dwarf galaxies of similar rotation velocity.

Figure 8 illustrates an essential property of the simulations presented in this Letter: outflows selectively remove low angular momentum gas from high redshift galaxies. The mean angular momentum of gas blown out of the virial radius of galaxy DG1 is plotted as a function of time (red triangles) and shown to be as much as ten times smaller than the mean angular momentum of all the baryons (blue) and dark matter (black) accreted at the same time and then retained within the virial radius of the galaxy at $z=0$. As the central region of a galaxy is being assembled at $z > 1.5$ its mass profile and angular momentum content is then directly affected. This scenario, that maximizes energy transfer to the DM and gas outflows in the regions that will become the center of the galaxy by $z=0$, is a natural consequence of the hierarchical assembly of galaxies in the CDM model.

The results described in the Letter confirm that energy transfer and subsequent gas removal in a clumpy ISM have the net effect of causing the central DM distribution to expand, while at the same time limiting the amount of baryons at the galaxy center. In Figure 5 we quantify this flattening by showing that by the present time the DM central profile in galaxies DG1 and DG2 is well approximated by a power law with slope α in the $-(0.5-0.7)$ range. These values of α are significantly flatter than in the collisionless control run and are in agreement with those of observed shallow DM profiles in dwarf galaxies^{13,14,64}.

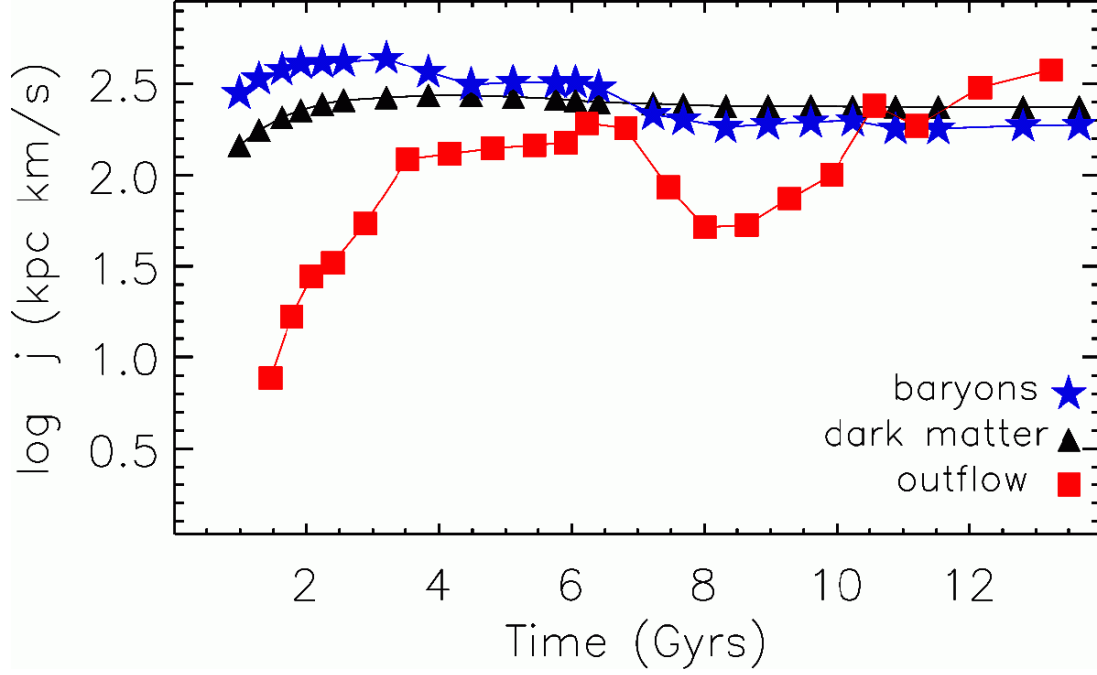


Figure 8. The angular momentum per unit mass of the DM and gas being accreted and of the gas being blown out as a function of time. While most of the matter accreted onto the galaxy halo has a fairly constant angular momentum, the gas being blown out at high redshift has a systematically lower angular momentum, by as much as an order of magnitude. During the same epoch and until $z=1$ the SFH of the galaxy is quite bursty. The stronger bursts are closely associated with epochs where the baryon distribution is clumpier and with decreases of the central DM density, supporting models^{8,15} for the formation of the DM core and the formation of bulgeless galaxies.

This result also resolves the dichotomy between CDM predictions of cuspy profiles based on DM-only runs^{46,57} and observations: neglecting the modeling of gas outflows suppresses the removal of DM matter from the galaxy center and makes the formation of shallow profiles impossible. The central concentration of mass in DG1LT, in which outflows are suppressed (Figure 5) and DM adiabatically contracts rather than expanding, results in the very steep inner rise of the rotation curve, followed by a steep decline. Such declining rotation curves are unrealistic in small galaxies and have long plagued hydrodynamical galaxy formation simulations. By looking at smaller, but well resolved halos formed in the high resolution region of our simulations (but outside the virial radius of the main galaxies) we verified that star forming galaxies with rotational velocity $V_{rot} \sim 30 \text{ km s}^{-1}$ also have shallow DM profiles, while even smaller dark galaxies (where SF was completely suppressed due to the gas heating by the cosmic UV field) have steep central DM profiles. This result confirms that gas outflows caused by SF feedback are the cause for the removal of low angular momentum gas and the formation of DM cores.

Received ; Accepted .

-
31. Wadsley, J., Stadel, J., & Quinn, T., Gasoline: a flexible, parallel implementation of TreeSPH. *New Astr.* **9**, 137-158 (2004)
 32. Barnes, J., & Hut, P., A Hierarchical O(NlogN) Force-Calculation Algorithm. *Nature* **324**, 446-449 (1986)
 33. Ding, H.-Q., Karasawa, N. and Goddard, III, W. A. The reduced cell multipole method for Coulomb interactions in periodic systems with million-atom unit cells. *CPL*, **196**, 6 (1992)
 34. Gingold, R.A. & Monaghan, J.J. Smoothed particle hydrodynamics: theory and application to non-spherical stars. *Mon. Not. R. Astron. Soc.* **181**, 375-389 (1977)
 35. Monaghan, J.J., Smoothed particle hydrodynamics. *Annual. Rev. Astron, Astrophys.* **30**, 543-574 (1992)
 36. Alvarez, M.A., Shapiro, P., Kyungjin A. & Iliev, I.T. Implications of WMAP 3 Year Data for Sources of Reionization. *Astrophys. J.* **644** L101-L104 (2006)
 37. Mateo, M., Dwarf Galaxies of the Local Group. *Annual Review of Astronomy and Astrophysics.* **36**, 435-506 (1998)
 38. Springel, V., & Hernquist, L. Cosmological smoothed particle hydrodynamics simulations: the entropy equation. *Mon. Not. R. Astron. Soc.* **333**, 649-664 (2002)
 39. Balsara, D.S., von Neumann stability analysis of smoothed particle hydrodynamics: suggestions for optimal algorithms. *J.Comput. Phys.* **121** 357-372 (1995)
 40. Tasker, E. J. and Bryan, G. L. The Effect of the Interstellar Model on Star Formation Properties in Galactic Disks. *Astrophys. J.* **673**, 810-831 2008.

41. Stinson, G. Seth, A. Katz, N. Wadsley, J. Governato, F. Quinn, T. Star formation and feedback in smoothed particle hydrodynamic simulations - I. Isolated galaxies *MNRAS*, **373**, (2006)
42. Hoeft, M., Yepes, G., Gottlöber, S. and Springel, V. Dwarf galaxies in voids: suppressing star formation with photoheating. *Mon. Not. R. Astron. Soc.* **371**, 401–414, 2006
43. Verde, L. et al. First-Year Wilkinson Microwave Anisotropy Probe (WMAP) Observations: Parameter Estimation Methodology. *Astrophys. J. Suppl.*, **148**, 195-211. (2003)
44. Katz, N. and White, S. D. M. Hierarchical galaxy formation - Overmerging and the formation of an X-ray cluster. *Astrophys. J.*, **412**, 455-478. (1993)
45. Power, C., *et al.*, The inner structure of Lambda CDM haloes - I. A numerical convergence study. *Mon. Not. R. Astron. Soc.* **338**, 14-34 (2003)
46. Diemand, J., Kuhlen, M. and Madau, P. Formation and Evolution of Galaxy Dark Matter Halos and Their Substructure. *Astrophys. J.*, **667** 859-877 (2007).
47. Jonsson, P., Groves, B. and Cox, T. J. High-Resolution Panchromatic Spectral Models of Galaxies including Photoionisation and Dust. astro-ph/0906.2156 (2009)
48. Adelman-McCarthy, J. K. et al., The Fourth Data Release of the Sloan Digital Sky Survey, *ApJS*, **162**, 38-48 (2006)
49. Peng, C. Y., Ho, L. C, Impey, C. D. and Rix, H. W., Detailed Structural Decomposition of Galaxy Images, *Astron. J.*, **124**, 266-293 (2002)
50. Begeman, K. G., H I rotation curves of spiral galaxies. I - NGC 3198 *Astron. Astrophys.*, **223**, 47-60 (1989).
51. Rhee, G., Valenzuela, O., Klypin, A., Holtzman, J., and Moorthy, B., The Rotation Curves of Dwarf Galaxies: A Problem for Cold Dark Matter? *Astrophys. J.*, **617**, 1059, 1076 (2004)
52. Oh, S.-H., de Blok, W. J. G., Walter, F., Brinks, E. and Kennicutt, R. C., High-Resolution Dark Matter Density Profiles of THINGS Dwarf Galaxies: Correcting for Noncircular Motions *Astron. J.*, **136**, 276 (2008)
53. Mayer, L., Governato, F. and Kaufmann, T. The formation of disk galaxies in computer simulations *Advanced Science Letters* **1** 7-27 (2008).
54. Zavala, J. Okamoto, T. and Frenk, C. S. Bulges versus discs: the evolution of angular momentum in cosmological simulations of galaxy formation. *Astrophys. J.* **387**, 364-370 (2008)
55. Scannapieco, C., Tissera, P. and White, S. D. M. Effects of supernova feedback on the formation of galaxy discs *Mon. Not. R. Astron. Soc.* **389**, 1137-1149 (2008).
56. Bullock, J., Dekel, A., Kolatt, T. S., Kravtsov, A. V., Klypin, A. A., Porciani, C. and Primack, J. R. A Universal Angular Momentum Profile for Galactic Halos. *Astrophys. J.*, **555**, 240-257 (2001)

57. Springel, V., Wang, J., Vogelsberger, M., Ludlow, A., Jenkins, A., Helmi, A., Navarro, J. F., Frenk, C. S. and White, S. D. M. The Aquarius Project: the subhaloes of galactic haloes. *Mon. Not. R. Astron. Soc.*, **391**, 1685–1711 (2008).
58. Bate, M. R. and Burkert, A., Resolution requirements for smoothed particle hydrodynamics calculations with self-gravity. *Mon. Not. R. Astron. Soc.* **288**, 1060-1072 (1997)
59. Tonini, C., Lapi, A. and Salucci, P. Angular Momentum Transfer in Dark Matter Halos: Erasing the Cusp. *Astrophys. J.*, **649**, 591–598, 2006
60. El-Zant, A. A., Hoffman, Y., Primack, J., Combes, F., & Shlosman, I. Flat-cored Dark Matter in Cuspy Clusters of Galaxies *Astrophys. J. Lett.*, **607**, L75, 2004
61. Saitoh, T. R., Daisaka, H., Kokubo, E., Makino, J., Okamoto, T., Tomisaka, K, Wada, K. and Yoshida, N. Toward First-Principle Simulations of Galaxy Formation: I. How Should We Choose Star-Formation Criteria in High-Resolution Simulations of Disk Galaxies? *PASJ* **60**, 667 (2008)
62. Walter, F., Brinks, E., de Blok, W. J. G., Bigiel, F., Kennicutt, R. C., Thornley, M. D. and Leroy, A. THINGS: The H I Nearby Galaxy Survey. *Astron. J.*, **136** 810–2125 (2008)
63. Blanton, M. R., Geha, M. and West, A. A. Testing Cold Dark Matter with the Low-Mass Tully-Fisher Relation *Astrophys. J.*, **682**, 861–873 (2008).
64. Flores, R. A., & Primack, J. R. Observational and theoretical constraints on singular dark matter halos *Astrophys. J. Lett.*, **427**, 1–4, (1994)

7 Supplementary Notes

FG acknowledges support from HST GO-1125, NSF ITR grant PHY-0205413 (also supporting TQ), NSF grant AST-0607819 and NASA ATP NNX08AG84G. CBB acknowledges the support of the UK’s Science & Technology Facilities Council (ST/F002432/1). PJ was supported by programs HST-AR-10678 and 10958 and by Spitzer Theory Grant 30183 from the Jet Propulsion Laboratory. LM was supported by a grant of the Swiss National Science Foundation. LM and CB thank the Kavli Institute for Theoretical Physics at UC Santa Barbara for hospitality during completion of the work. We thank the computer resources and technical support by TERAGRID, ARSC, NAS and the UW computing center, where the simulations were run.

8 Supplementary Movie Legend

The movie shows the evolution of the gas density (in blue) in the region where galaxy DG2 forms, from shortly after the Big Bang to the present time. The frame is 15 kpc per side. Brighter colors correspond to higher gas densities. The movie highlights the numerous outflows that remove low angular momentum gas and the connection between outflows with accretion and early merger events.